Organo Opto-Electronics
An International Journal

http://dx.doi.org/10.12785/ooe/010104

Dielectric and Electric Modulus Studies on Ni (II) Tetraphenyl Porphyrin Thin Films

***Ahmed M. Nawar*[1,*], *H. M. Abd El-Khalek*[1] *and M. M. El-Nahass*[2]**

[1]Thin Film Laboratory, Physics Department, Faculty of Science, Suez Canal University, Ismailia, Egypt.
[2]Thin Film Laboratory, Physics Department, Faculty of Education, Ain Shams University, Heliopolis, Roxy, Cairo, Egypt.

Received: 08 Feb 2015, Revised: 22 March 2015, Accepted: 10 Apr 2015
Published online: 01 July 2015

Abstract: Ni (II) tetraphenyl porphyrin, NiTPP, thin films were successfully prepared by using thermal evaporation technique. The dielectric properties and AC conductivity of thermally evaporated Au/NiTPP/Au thin films are investigated as function of temperature (303-443K) and frequency (42Hz-5MHz). The AC conductivity is found to obey Jonschers universal power law, $\sigma_{ac}(\omega)=A\omega^{s}$, ($\omega$ is the angular frequency). The correlated barrier hopping is found to be the dominant conduction mechanism for charge carrier transport. The behavior of the real and imaginary parts of the dielectric constant is discussed as a function of both temperature and frequency. The scaling behaviour of imaginary part of electric modulus suggests that the relaxation describes the same mechanism at various temperatures in NiTPP thin films. The Cole-Cole diagram determined complex electric modulus and the static, ε_s, and dynamic, ε_∞, dielectric constants of NiTPP thin films were determined for different temperatures. The calculated capacitance of the grain boundary, C_g, and the static dielectric constant are found to be increasing with the temperature. The calculated resistance of the grain boundary, R_g, and the dynamic dielectric constant are found to be deceasing with the increasing of temperature.

Keywords: Organic thin films, Dielectric properties, Electric modulus, Static and Dynamic dielectric constants.

1 Introduction

The emerging field of organic semiconductor materials and devices is extending the capabilities and possibilities of modern electronic and photonics into unexpected domains. Characterizations of organic semiconductors in thin film form are important for pure and applied sciences because of their potential use in electronics and instrumentation industry. Among this group of materials, organic molecules with conjugated electron systems, such as porphyrin molecules, have created a new class of materials that offer the possibility of implementing innovative applications in many modern applications. Porphyrin dyes or so called pigments of life are important chromophores which play an essential function in many biological processes ranging from oxygen transport to photosynthesis, from catalysis to pigmentation changes and in optoelectronic techniques, in laser sciences and in electronic devices [1,2]. The dielectric properties of a material have an important role in the performance of the device. It is well known that a successful dielectric material must have low dielectric constant, low dielectric loss, and high breakdown voltage. The dielectric constant relates to the polarizability of a material and is therefore strongly dependent on chemical structure [3,4].

Considerable progress has been made since the early days of Cole and Cole [5], in utilizing complex plots and frequency explicit plots to explain the dielectric behaviour and electrical conductivity of a wide range of solid state materials [6]. One of the main advantages of frequency-dependent measurements is that the contributions of the bulk material, the grain boundaries and electrode defects can easily be separated if the time constants are different enough [7] to allow separation. Impedance spectroscopy (IS) is a relatively new and powerful method of characterizing many of the electrical properties of materials and their interfaces with electronically conducting electrodes. It may be used to investigate the dynamics of bound or mobile charge in the bulk or interfacial regions of any kind of solid or liquid material: ionic, semiconducting, mixed electronicionic and even insulators (dielectrics). Dielectric measurements are an important means for studying the dynamic properties (capacitance, conductance, permittivity and loss factor) of a dielectric. The advantage of ac measurements over the dc measurements is that internal time-dependent processes in the

* Corresponding author e-mail: nawarphysics@yahoo.com Ahmed_Nawar@science.suez.edu.eg

insulator can be investigated with ac measurements. Moreover, the ac voltage bias need never exceed a few hundred millivolts, thus the maximum field within the sample is kept to a minimum and there is little danger of more than one conduction process being active [8]. The scope of this study is the analysis of the dielectric properties of thermally evaporated Ni (II) tetraphenyl porphyrin thin films sandwiched between two gold electrodes (ohmic contact). Particular emphasis is placed on the effects of the thermal annealing of the as-evaporated films, static and dynamic dielectric constants are investigated. The data were analyzed within three different formalisms, those of complex permittivity, ε^*, complex electric modulus, M^* and complex impedance, Z^* to extract the maximum amount of information from the experimental data [9].

2 Experimental techniques

A dark purple crystalline powder 5, 10, 15, 20-Tetraphenyl-21H, 23H-porphine nickel (II) NiTPP was purchased from Aldrich Chem. Co. and was used as was received without any further purification. Thin films of NiTPP with thickness 650 nm were prepared by thermal evaporation technique, using a high vacuum coating unit (Edward, E 306 A, England), under a pressure of about 2×10^{-5} Torr. A suitable quartz crucible was heated slowly by a tungsten coil and used for evaporating the NiTPP powder. The rate of deposition was controlled to be 2 nm/second using a quartz crystal thickness monitor (Edwards, Model FTM4). The deposited NiTPP thin films were sandwiched between two gold electrodes for electrical measurements; the gold contacts were tested to be ohmic. The gold electrodes with a thickness of about 100 nm were thermally evaporated directly from boat-shaped molybdenum filament.

The differential thermal analysis (DTA) measurement was carried out by the Shimadzu instrument (DTA-50) calibrated through the melting points of indium and tin. The thermal gravimetric analysis (TGA) was recorded using the (TGA-50) system in the presence of air for NiTPP in powder form, within the temperature range from room temperature to 1073 K. The thermal measurements were repeated twice and values agreed within the experimental errors ±1 K. The chemical structure of NiTPP material was characterized in powder, as grown NiTPP thin films and annealed NiTPP thin films in roughing vacuum at 573 K under roughing vacuum at 10^{-3} Pa with soaking time of three hours thin film forms by FTIR technique, by using a Bruker, Vector 22 spectrometer in the range from 4000 to 400 cm^{-1}.

A programmable automatic RLC bridge, model HIOKI 3531-Hi-tester LCR meter with a test fixture model HIOKI 3531 was used to measure the impedance, Z, loss tangent, tanδ conductance, G_p, and capacitance, C_p, directly in the frequency ranging from 42 Hz to 5MHz, with an oscillation level of 0.5 V and the data were recorded with a delay time 0.05 Sec. The dielectric properties are investigated under dark conditions using a special designed holder. The temperature was controlled with a programmable oven with the temperature range 303373K with accuracy of about ±1 K.

It is known that the dielectric permittivity is expressed as a complex number $\varepsilon^*(\omega)=\varepsilon^{'}(\omega)-i\varepsilon^{''}(\omega)$, where the real part, $\varepsilon^{'}(\omega)$, is the relative permittivity or dielectric constant and the imaginary part, $\varepsilon^{''}(\omega)$, represents the loss factor as a functions in angular frequency, $\omega$and The dielectric constant, $\varepsilon^{'}$, was calculated as follows:

$$\varepsilon^{'}(\omega)=\frac{C_p d}{\varepsilon_o A} \tag{1}$$

where d is the thickness of the films and A the area of cross section of the film. The imaginary part of the dielectric constant, $\varepsilon^{''}$, is calculated using the relation:

$$\varepsilon^{''}(\omega)=\varepsilon^{'} tan\delta \tag{2}$$

The real part, $Z^{'}(\omega)$, and imaginary part, $Z^{''}(\omega)$, of the complex impedance were calculating as follows:

$$Z^{'}(\omega)=\frac{G_p}{G_p^2+\omega^2C_p^2} \tag{3}$$

$$Z^{''}(\omega)=\frac{G_p\omega}{G_p^2+\omega^2C_p^2} \tag{4}$$

where G_p and C_p are the measured parallel conductance and the capacitance and the angular frequency is given by $\omega=2\pi f$.

3 Results and discussion

3.1 Structure characterizations

TGA analysis is widely used to evaluate the thermal stability of the organic materials [10]. In order to determine the decomposition and sublimation temperature of NiTPP in powder form as purchased without any purification, the

thermogravic analysis (TGA) and (DTA) curves of NiTPP in powder form taken at a heating rate of 10°C/min are shown in Fig. 11 as the beginning of detection of weight loss. Also, $T_{1/2}$ was established as the temperature at which the sample had lost a half of the initial weight. Between these two temperature values, sublimation of powder occurred. In the present case, the beginning of weight loss at T_i, and is due to the sublimation of NiTPP solid powder. These curves show that NiTPP has a thermal stability up to approximately 700 K, increasing the temperature above this degree causing a sublimation of the material from the solid into the gas vapour molecules [11,12].

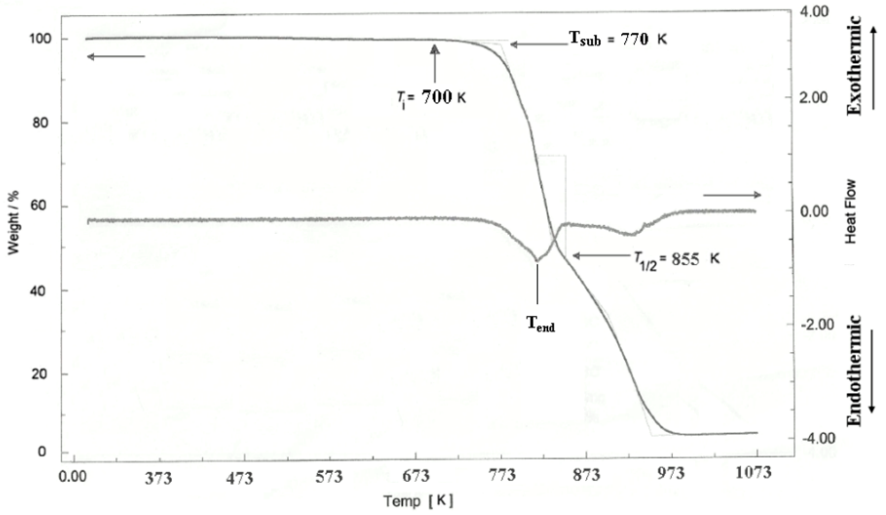

Fig. 1: Thermogravic curves of powder NiTPP at 0.167 K. s^{-1} and the initial weight of the Sample was 7.627 mg.

This study indicates that the compound could be used in its solid form for any application up to 700 K. The obtained curve from DSC measurement is shown in the same figure; no exothermic calorimetric signals were detected at the decomposition temperatures, determined from the previous thermogravimetric experiment, nor before the melting point. Perlovich et al. [11] in their study of the thermodynamics of porphyrin sublimation have mentioned that metallo-complexes of tetraphenyl porphyrin by DSC showed that there are well-reproduced endothermal peaks on the thermograms which correspond to Metallo-TPP fusion [12]. The values for the enthalpies and temperatures of melting were not provided. There are not many organic molecules that show this feature. The condensation of pyrrole and methine groups will afford the remarkable stability to the porphyrin macrocycle, which sublimate at T ≈ 770 K. The value of sublimation temperature of NiTPP reflects that the inclusion of the metallic ion in the macrocycle improves the thermal stability in the metalloporphyrins [12]. The endothermic temperature, T_{end}, is correlated with the sublimation of NiTPP material.

The chemical structure of the powder, the as-deposited and annealed films was investigated by Fourier Transform Infrared technique. Fig. 2 illustrates FT-IR spectra in the range 400-4000 cm^{-1} acquired from fresh NiTPP powder in comparison with spectra corresponding to as-deposited and annealed films of thickness 650 nm. Inspection of this figure reveals that the thermal evaporation technique is a good one to obtain undissociated and stoichiometric NiTPP films [13]. In addition, the spectrum of the annealed film is also quit similar to that of the powder and the as-deposited film, which revealed that a NiTPP film has a thermal stability up to the used annealing temperature. The observed FT-IR bands and their assignments are listed in Table (1), which are in a good agreement with that in literature [14,15,16,17,18]. The effects of annealing temperatures on the morphological, structural and optical properties have been investigated up to 573 K [19].

Dielectric and AC conductivity studies The real part of the dielectric constant, $\varepsilon'(\omega)$, is related to the capacitive nature of the material and is a measure of the reversible energy stored in the material by polarization, whereas $\varepsilon''(\omega)$ is a measure of the energy required for molecular motion, that is the energy dissipated in this motion in the presence of an electric field, divided into relaxation and conductivity contribution (energy required to align dipoles and move ions) [20, 21]. The dependence of $\varepsilon'(\omega)$ on the frequency and temperature of Au/NiTPP/Au device is shown in Figs. 3(a) and 3(b). A comparative study of these figures indicates that the value of $\varepsilon'(\omega)$ decreases with the increase both of frequency and temperature except of the MHz region, the rate of the decrease in $\varepsilon'(\omega)$ by rising temperature is faster at lower and

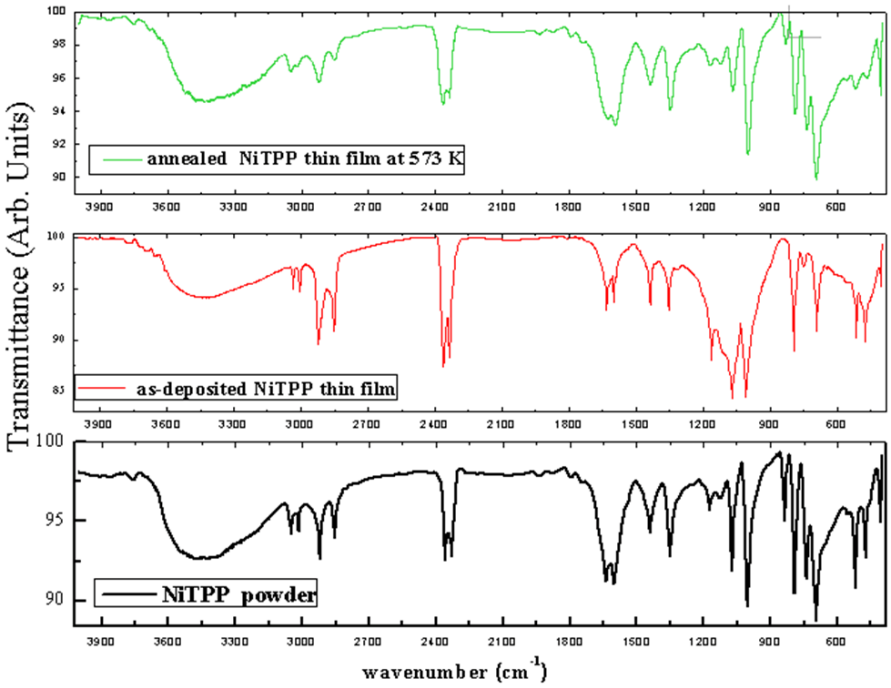

Fig. 2: FT-IR spectra of NiTPP in different forms; powder, as deposited film, and annealed film at 573K for 3h.

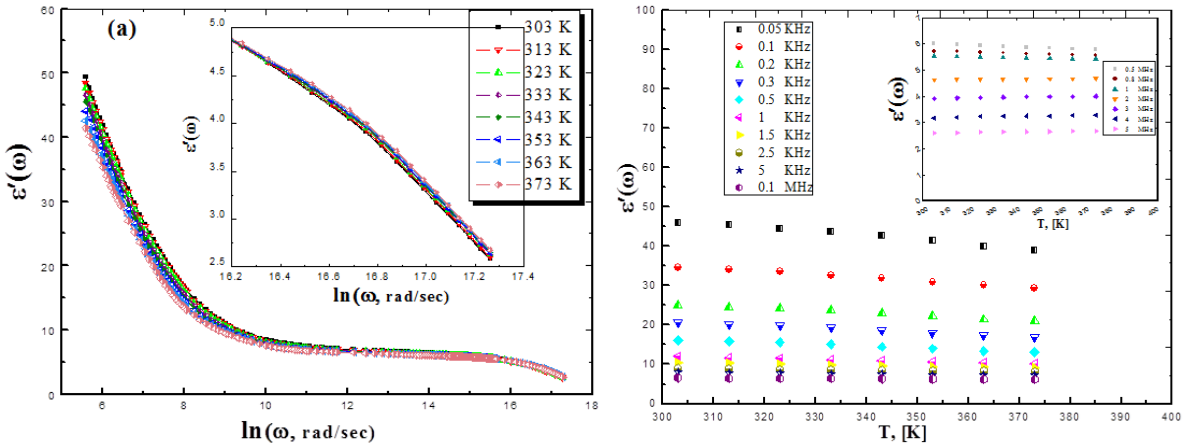

Fig. 3: (a) Shows the frequency dependence of the real part of the dielectric constant, $\varepsilon^{'}(\omega)$, for NiTPP films at different temperatures. (b) Shows the temperature dependence of the real part of the dielectric constant, $\varepsilon^{'}(\omega)$, for NiTPP films at different frequencies.

intermediate frequencies. In MHz region the inset in Fig. 3(a) reveals that the temperature enhances the dielectric constant by a very small rate.

The decrease of $\varepsilon^{'}(\omega)$ with the increase e of frequency can be explained as follows; in carrier-dominated dielectric materials, the value of $\varepsilon^{'}(\omega)$ is high at low frequencies, and shows frequency dispersion due to space-charge polarization. In dielectric NiTPP films, interfaces with a large volume fractions, which may be contain a large number of defects, such as dangling bonds, vacancies, vacancy clusters, and micro porosities, which can cause a change of positive and negative space charge distribution in interfaces. When subjected to an electric field, these space charges move. When they are trapped by defects, lots of dipole moments are formed [22,23]; it means that the region of lower frequencies have a

Table 1: IR spectral data in different forms; powder, as-deposited and annealed NiTPP films.

Wave number (cm^1)			Assignment
Powder	As-deposited film	Annealed- film	
3424	3426	3425	(-OH) is associated, certainly, with the water absorbed by KBr from the atmosphere.
(2919-2329)	(2917-2332)	(2922-2331)	ν (C-H) (aromatic)
1636.2	1629.3	1632.3	$\nu(C_a\text{-}C_m)_{asym.}$
1600	1599	1597.3	ν(C-N)
1436	1436.6	1437	phenyl
1349	1351	1350.7	ν(C-N)
1158.4	1158.2	1159.2	$\nu(C_m\text{-H})$
1123.6	–	1124	$\delta(\text{Cb-H})_{asym.}$
1068.3	1066.6	1069.1	$\nu(\text{Cb-H})_{asym.}$
1000.2	1004	1003	ν(pyr. breathing)
834.1	–	835.4	δ (Pyr. deform)$_{asym.}$
789.6	792	791.8	δ (Pyr. deform)$_{asym.}$
696.8	697.6	696.3	$\gamma(\text{Cb-H})_{sym.}$
516	515.7	514.6	phenyl
467.7	468.5	468.2	δ (Pyr rot.)
404.4	405.5	403.3	δ (Pyr rot.)

*Abbreviation: sym. =symmetrical; asym. = asymmetrical, the ν, δ, γ denote stretching, in-plane bending and out-of-plane bending modes, respectively.

permanent dipoles which can align themselves along the direction of the field and contribute to the total polarization of the dielectric material.

On the other hand, at higher frequency the variation in field is too rapid for the dipoles to align themselves in the direction of field, i.e., dipoles can no longer follow the field, so their contribution to the total polarization and hence to the dielectric constant become smaller. In MHz region, the charge carriers would barely have started to move before the field reversal occurs and $\varepsilon^{'}(\omega)$ falls to a small value at higher frequencies in NiTPP films [23,24].

In the case of NiTPP films, the dielectric constant, $\varepsilon^{'}(\omega)$, decreases with increasing temperature ranging from 303 to 373 K, this phenomenon is explained based on space charge polarization and reversal of the direction of polarization [26]; as the temperature increases the volume of granular particles, V_g, increases, and the interfaces volume, V_i, gradually decrease. When V_g increases the contribution to $\varepsilon^{'}(\omega)$ by electronic relaxation polarisation appearing mainly inside the particles increases, but due to the decrease in the value of V_i, the contribution to $\varepsilon^{'}(\omega)$ by space charge polarisation and rotation of the direction of polarisation occurring mainly in interfaces diminishes. As a result $\varepsilon^{'}(\omega)$ decreases with increasing temperature as the particle size increases.

The same behavior of decreasing dielectric constant with increasing temperature was reported in [26,27,28,29]. The inset of in Fig. 3(b) reveals a slight increase in the values of $\varepsilon^{'}(\omega)$ in MHz region, may be explained as follow; at the same temperature, the higher frequencies enhances the induced polarization inside V_g which in turn becomes larger than the total induced polarization of V_g and V_i at the this temperature. As a result of increasing temperature and frequency the increase in the induced polarization inside V_g substitutes the loss due to diminish of V_i and the values of $\varepsilon^{'}(\omega)$ increases, slightly, from the lower temperature to the next higher one. The previous discussed behaviour may be useful in the microelectronics industry, it is required to replace the dielectric materials in multilevel interconnect structures with low dielectric constant materials as an interlayer dielectric (ILD), which surround and insulate interconnect wiring. Lowering the dielectric constant values of the ILD decreases the RC delay, lowers power consumption and reduces cross-talk between nearby interconnects [30].

The dielectric loss, $\varepsilon^{''}(\omega)$, was measured as a function of frequency and temperature. Figures 4(a) and 4(b) show the dependence of $\varepsilon^{'}(\omega)$ on the frequency and temperature, respectively. It is observed from the figures that $\varepsilon^{'}(\omega)$ is found to decrease with the increase in frequency and increases with the increase in temperature in lower and intermediate frequencies. The origins of the dielectric losses are the conduction losses, dipole losses and vibrational losses [31,32]. As the temperature increases, σ_{ac} increases, and the electrical conduction losses increase and hence increases the value of the dielectric loss, $\varepsilon^{''}(\omega)$. The conduction losses usually increase with the increment in the DC conductivity towards high temperatures. The insets of previous figures 4(a) and 4(b) reveal that the contribution of DC conductivity was eliminated at high angular frequencies larger than 200 KHz to 5 MHz region and the dielectric loss increases with frequency and decreases with increasing temperature.

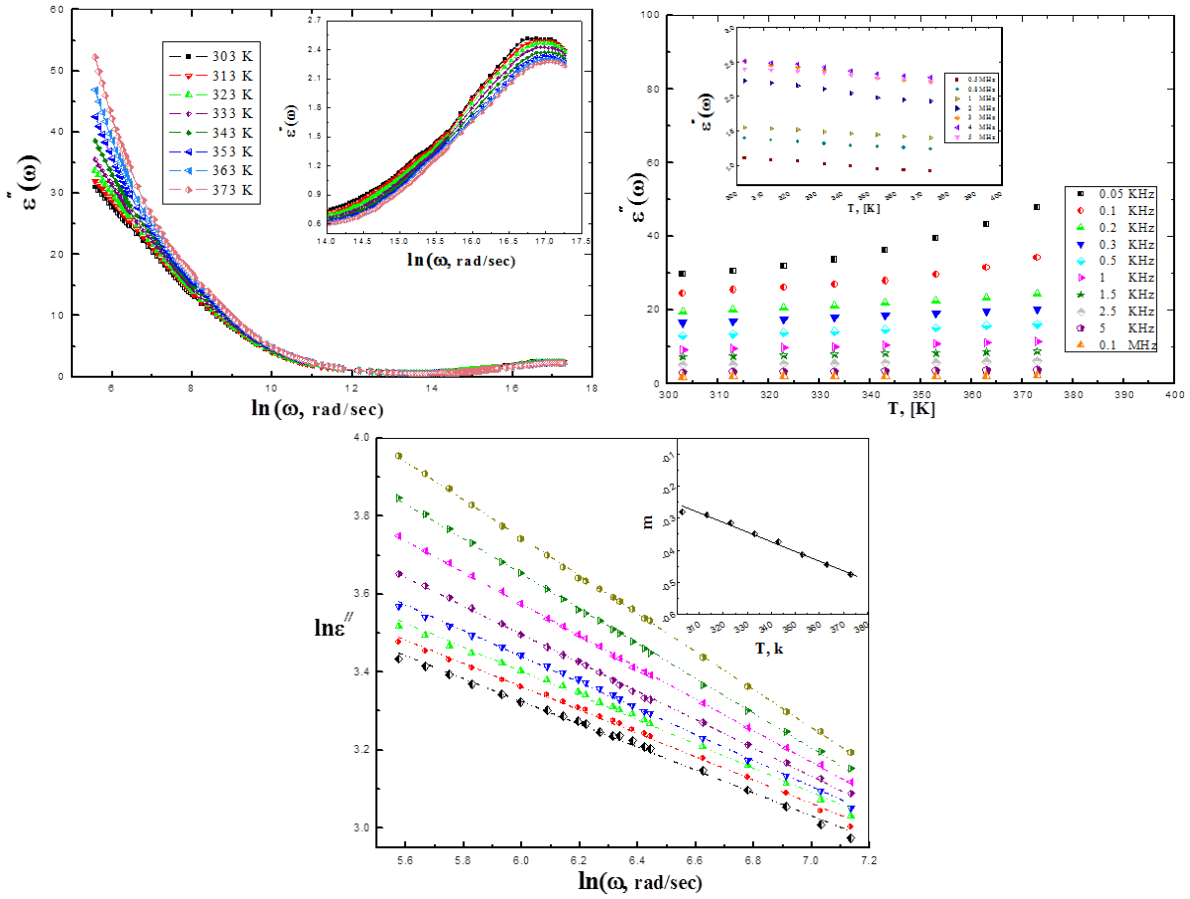

Fig. 4: (a) Shows the frequency dependence of the imaginary part of the dielectric constant, $\varepsilon''(\omega)$, for NiTPP films at different temperatures, (b) Shows the temperature dependence of the imaginary part of the dielectric constant, $ln\varepsilon''(\omega)$, for NiTPP films at different frequencies (c) Shows the variation of $ln\varepsilon''(\omega)$ with $\ln\omega$ for NiTPP films at different temperatures. The inset shows temperature dependence of the parameter (m).

According to Giuntini et al. model [33], the dielectric loss $\varepsilon''(\omega)$ at a particular frequency in the temperature range is given by the following equation:

$$\varepsilon'' = 2\pi^2 N(\varepsilon_s - \varepsilon_\infty)\left[\frac{ne^2}{\varepsilon_s}\right]^3 k_B T \tau_o^m W_M^4 \omega^m \tag{5}$$

and

$$m = -\frac{4k_B T}{W_M} \tag{6}$$

This can be written as;

$$\varepsilon'' = B\omega^m, \tag{7}$$

where ε_s and ε_s are the static and optical dielectric constants, respectively, N is the concentration of the density states, n is the number of electrons that hop and W_M is the maximum barrier height (the energy required to move the electron from a site to the infinity). The power (m) can be calculated from the slope of the obtained straight lines of Fig. 4(c). From the above Eq. (6), the power, m, should be negative and decreases with increasing temperature showing a linear behavior, which is confirmed in the inset of Fig. 4(c) the investigated values of (m) are comparable with those obtained for organic material [26] by this model. The calculated values of WM were found to be decreased from 0.37 to 0.27 eV as the temperature increased from 303 to 423 K.

The study of angular frequency dependent conductivity is a well established method for characterizing the hopping dynamics of the charge carrier/ions. The angular frequency dependence of AC conductivity is usually characterized by

Jonschers power law features [34].

$$\sigma_{ac}(\omega) = A\omega^{s}, \tag{8}$$

where A is a temperature-dependent constant, ω the angular frequency, $\omega = 2\pi f$ and s is the frequency exponent in the range $0 < s < 1$, which can be determined from the measured results.

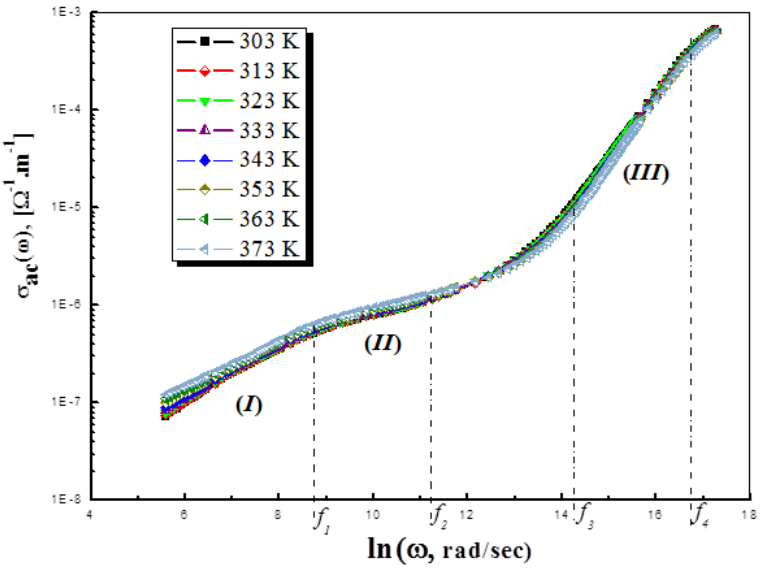

Fig. 5: Shows the frequency dependence on AC conductivity, σ_{AC}, at various temperatures for NiTPP films.

Fig. 5 shows a typical frequency dependence of AC conductivity for NiTPP device at different temperatures, the angular frequency dependence of conductivity exhibiting both low and high frequency dispersion. It is clear that the conductivity spectra have Jonschers power law features, Four threshold frequencies f_1, f_2, f_3 and f_4 separating the entire variation into three regions: (I) low frequencies region at $f < f_1$; the conductivity increases linearly with the frequency. The values of s are obtained by fitting $\ln\sigma(\omega, T)$ versus $\ln\omega$ plots in this region, the exponent s is less than unity, $0.674 > s > 0.533$, and decreases with the increase in temperature.

The decrease of s with the increase in temperatures has been observed by Al-Ddhhan and Hogarth [34] for amorphous oxide films. Similar measurements of s were also obtained for α-CuPc thin films with ohmic electrodes, where the s values were found to be less than unity and decreased with the increase in temperature [35]. These results are in agreement with the previous works for organic sandwiched thin films [36,37]. The inset figure shows that the value of s increases with decreasing temperature and approaches 0.674 at 303 K. This reveals that the conduction mechanism in this region corresponds to the correlated barrier hopping model, which is the most suitable model to describe the AC electrical conduction for NiTPP thin films in the temperature range from 303 to 423 K.

In region (II) Moderate frequencies region, f_1 $f < f_2$, the conductivity increases linearly with the frequency. The values of s are obtained by fitting $\ln\sigma(\omega, T)$ versus $\ln\omega$ plots in this region, which are found to be decreased from 0.32 to 0.28, i.e. $0 < s < 1$. This result indicates that the conduction mechanism in this region still corresponds to the correlated barrier hopping model. (*III*) High frequencies region, f_3 $f < f_4$, where the conductivity increases linearly with the frequency. In this region s values increases from 1.44 to 1.52, i.e. $1 < s < 2$. This reveals that the conduction mechanism in this range of frequencies may be corresponded to the well-localized hopping and/or reorientational motion [38,39,40,41,42].

3.2 Electric modulus formalism

The dielectric properties can be analyzed via complex electric modulus formalism $M^*(\omega)$ and is another important characteristic in a thin film; where the electrical transport process parameters (the electrical and dipolar relaxation time and its activation energy, etc.) [43,44,45]. A comparison of the experimental data in the $M^*(\omega)$ and the $\varepsilon^*(\omega)$ representation is very useful to distinguish long-range conduction processes from localized dielectric relaxation [46]. It

is also suitable to extract phenomena such as electrode polarization [44] in the Au/NiTPP/Au sandwiched films under investigation. The analysis of dielectric dispersion data becomes more difficult in the absence of a well-defined dielectric loss $\varepsilon^{''}(\omega)$ peak, so that, another analysis or method is required to find the electrical transport process parameters in solids [49]. We focused in this work on the analysis of dielectric properties of Au/NiTPP/Au films by using complex electric modulus plots which can give more importance to elements with the smallest capacitance occurring in the dielectric system [50]. The electric modulus $M^*(\omega)$ as expressed in the complex modulus formalisms are defined by [47, 48]:

$$M^*(\omega) = \frac{1}{\varepsilon^*(\omega)} = \frac{1}{\varepsilon^{'}(\omega) + \varepsilon^{''}(\omega)} \tag{9}$$

$$M^*(\omega) = M^{'}(\omega) + jM^{''}(\omega), \tag{10}$$

$$M^{'}(\omega) = \frac{\varepsilon^{'}}{(\varepsilon^{'})^2 + (\varepsilon^{''})^2}, \quad M^{''}(\omega) = \frac{\varepsilon^{''}}{(\varepsilon^{'})^2 + (\varepsilon^{''})^2} \tag{11}$$

where $M^{'}(\omega)$ and $M^{''}(\omega)$ are the real and imaginary parts of the electric modulus, respectively, j = $\sqrt{-1}$ and ω = angular frequency, 2πf. The dependence of real part, $M^{'}(\omega)$, and imaginary parts $M^{''}(\omega)$ of electric modulus on the angular frequency is depicted in Fig. 6 for Au/NiTPP/Au at different temperatures.

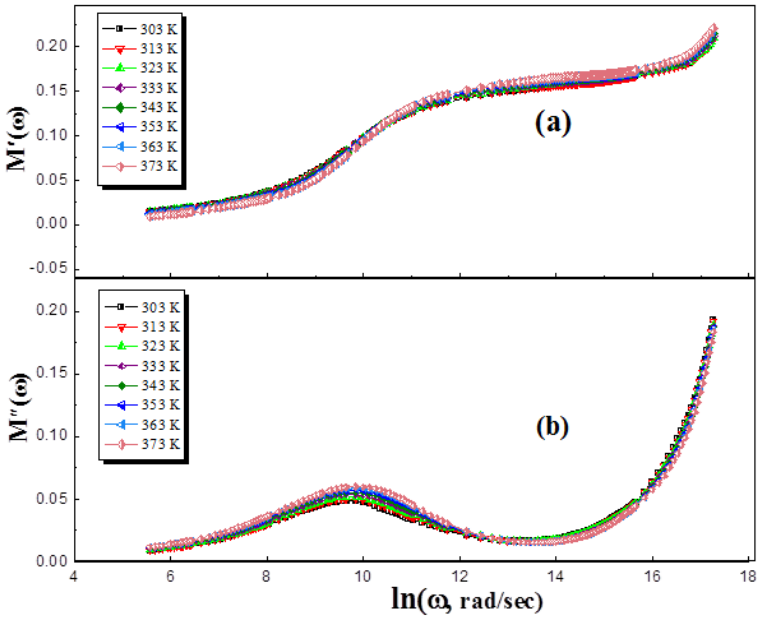

Fig. 6: Shows the variation of (a) real part, $M^{'}(\omega)$, and (b) imaginary part, $M^{''}(\omega)$, of the electric modulus versus lnω at various temperatures for Au/NiTPP/Au films.

Fig. 6(a) reveals that; the increase in temperature leads to a decrease in the value of $M^{'}(\omega)$ in the lower frequency range and increase its value at higher frequencies in MHz range. It is clear that $M^{'}(\omega)$ shows a dispersion behaviour tending towards M_∞, (M_∞= the asymptotic value of $M^{'}(\omega)$ at higher frequencies). At low frequencies, the electrode effects are dominant and $M^{'}(\omega)$ approaches to zero. It can be seen that the interfacial effects tend to be eliminated in modulus representation [51]. Fig. 6(b) shows that the peaks developed in the values of $M^{''}(\omega)$ indicate a relaxation process with increasing temperature and exhibits a maximum value, $M^{''}_{max}$, centred at the dispersion region of $M^{'}(\omega)$. The frequency region below peak maximum determines the range in which charge carriers are mobiles on long-range distances and above peak maximum, the carriers are confined to potential wells being mobile on short distances. At lower frequencies, $M^{''}(\omega)$ tends to be very small, confirming that the electrode effects make a negligible contribution and hence may be ignored when the data are analyzed in terms of modulus formalism [50].

The frequency dependence of modulus has been described by the (KohlraushWilliamsWatts) function ϕ(t), which describes the electric field decay [52]:

$$M^*(\omega) = \frac{1}{\varepsilon_\infty}\left[1 - \int_0^\infty exp(-j\omega t)\left(\frac{d\phi}{dt}\right)dt\right] \tag{12}$$

The peak of electric modulus can be analyzed by the following relation

$$\phi(t) = exp\left(\frac{-t}{\tau_M}\right)^\beta \tag{13}$$

where τ_M is the time at which $\phi(t)$ decays to (1/e) and the exponent β describes the breadth of the distribution in the limits of $0< \beta <1$. The τ_M and β parameters of the stretched exponential function are the conductivity relaxation time and the Kohlraush exponential function, respectively.

The stretching parameter, β=1.14/FWHM, has been calculated by extractthe full width at half-height, FWHM, by using Lorentzian fitting function of the modulus peak. The investigated β values for different samples are reported in Table (2); these values imply a non-Debye relaxation type for all temperatures. The average values of τ_M increasing by decreasing β.

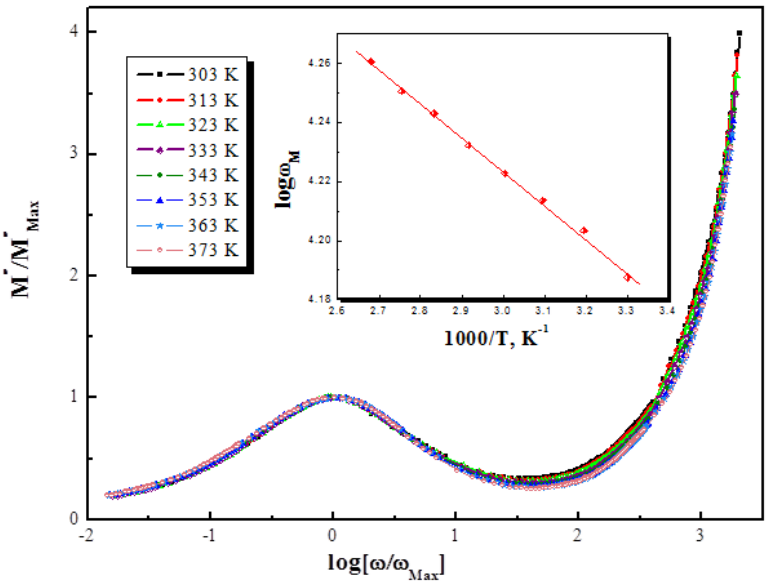

Fig. 7: Plots of the calculated values of (M''/M''_{max}) versus log (ω/ω_{max}) for NiTPP films at different temperatures. Inset: Arrhenius plot of the peak frequencies ω_M.

Fig. 7 shows plots of the calculated values of M''/M''_{max} versus log (ω/ω_{max}) for NiTPP devices at different temperatures; the overlapping of the curves for all the temperatures into a single master curve reveals that the dynamical processes are nearly temperature independent. The temperature dependence of the characteristic relaxation time is shown in the inset of Fig. 7, which satisfies the Arrhenius law given by: $\omega_M = \omega_o exp(-\Delta E_\tau/K_b T)$, where ω_o is the pre-exponential factor, k_b, is the Boltzmann constant, T is the characteristic temperature and E_τ is activation energy of the relaxation process.

The values of ω_M were determined from the maximum peak positions of Fig. 6(b) using $\omega_\tau = 2\pi f_M \tau = 1$ where f_M is the peak frequency, from the numerical fitting analysis the value of ΔE_τ was found to be 22.8 $\pm$ 2 meV for NiTPP films. The calculated values of $M'(\omega)$ and $M''(\omega)$ are investigated by ColeCole diagrams as shown in Fig. 8(a) at temperature ranging from 303 to 373 K. These semicircles would show to which category the NiTPP devices belongs; whether to a category where electric compliance is dominating or to a category where electric stiffness is dominating. Electric compliance, i.e. how easily dipoles are created and/or oriented in the solid, is represented by the permittivity

Table 2: The extracted dielectric parameters, capacitance and resistance of interior grain at different temperatures.

T [K]	Dielectric parameters						Interior Grain parameters		
	M'_∞	ε_∞	ε_s	$\Delta\varepsilon$	β	α	$\tau_M(10^{-4})S$	C_g nf	$R_g(K\Omega)$
303	0.1569	6.37	83.5	77.13	0.788	0.203	4.07	1.89	215.4
313	0.1589	6.29	98.04	91.75	0.754	0.244	3.93	2.26	174
323	0.16104	6.21	101.3	95.1	0.724	0.272	3.84	2.34	164.1
333	0.1621	6.17	115.2	109	0.706	0.285	3.76	2.68	140.2
343	0.1633	6.12	127.5	121.4	0.679	0.325	3.68	2.98	123.2
353	0.16471	6.07	155.1	149	0.656	0.351	3.59	3.66	97.9
363	0.16622	6.02	156.1	150.1	0.634	0.358	3.53	3.69	95.6
373	0.16623	6	164.7	158.7	0.613	0.348	3.44	3.9	88.1

$\varepsilon^*(\omega)$, whilst electric stiffness, i.e. with what difficulty dipoles are created and/or oriented in the solid, is represented by the electric modulus $M^*(\omega)$.

For the present NiTPP films, the electric modulus $M^*(\omega)$ was found as a dominating property of electric compliance according to Fig. 8(a). The peak frequency of $M''(\omega)$ shows a slight shifts towards the high frequency region as temperature increases, which implies conductivity relaxation suggesting that the dielectric relaxation, is activated thermally, in which a hopping process of charge carriers is predominant [53,54].

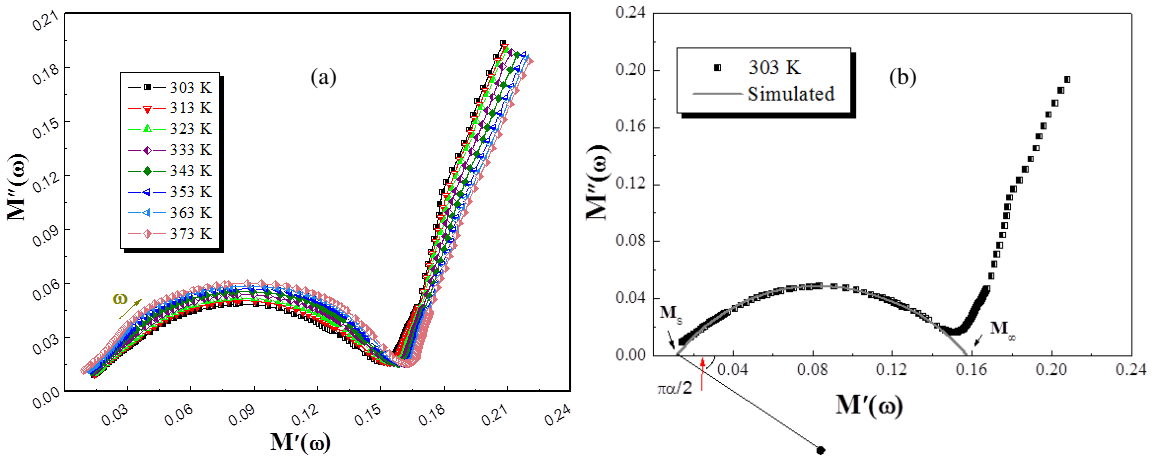

Fig. 8: Plots of imaginary part,$M''(\omega)$, versus real part, $M'(\omega)$,of electric modulus (a) at various temperatures for NiTPP films (b) at 303 K for NiTPP films, as a representation example.

At the low-frequency end (Fig. 8(a)), the formed semicircle does not reach the origin but has a small positive intersect on the $M'(\omega)$ axis, evidence of a dielectric relaxation process or of existing electrode polarization [55]. The increase in the values of $M'(\omega)$ and the subsequent development of $M''(\omega)$ peaks with increasing frequency is a characteristic behaviour of a dielectric dispersion. The constant value of $M'(\omega)$ at higher frequencies is due to the fact that interfacial polarization is ineffective at higher frequencies, as large dipoles developed at the interfaces cannot follow the electric field when the frequency is high. At the high-frequency end (Fig. 8(a)), another process starts which has been attributed to the orientation of dipolar groups [56-58]. The semicircle at the high-frequency end is a little skewed, and this deviation has also been observed in polystyrene glass beads composites [59].

It is most probable that this behaviour is connected with the start of a new process as already stated but it also expresses the asymmetrical character of the distribution of relaxation times. The capacitance values are calculated at the maximum frequency using the relation $M'' = C_o/2C_g$. The capacitance value is found to be in the range of Pico-Farad scale, which implies that the observed peak is due to the relaxation in bulk type components [60].

The static dielectric constant, $\varepsilon_S = 1/M_S$ and dielectric constant at high frequency, $\varepsilon_\infty = 1/M_\infty$, for NiTPP thin films can be determined by using the electric modulus $M^*(\omega)$ [53,61]. The most probable relaxation time is given by using the

following relation [54,62]:

$$(u/v) = (\omega_o \tau_M)^{1-\alpha} \tag{14}$$

where u is the distance on the ColeCole diagram between the experimental point, ω_o, and ε_S, the distance between that point and ε_∞ and the parameter α is equal to zero when the dielectric has only one relaxation time, whereas for a distribution of relaxation time it varies between 0 and 1 [63]. Fig. 8(b) with the aid of Eq. (11) illustrates a representative example for the ColeCole diagram at 303 K; a semicircle is obtained as shown in the figure. The centre of the semicircle lies below the abscissa axes by an angle$(\pi)/\alpha 2$. This confirms that there exists a distribution of relaxation times in NiTPP thin films.

According to the previous figure, the centred value, $M_c^{'} = M_\infty/2$, of the real part of $M^*(\omega)$ at τ_M is evaluated at the maximum value of $M^{''}(\omega)$ from the semicircle. The high frequency dielectric constant, $\varepsilon_\infty = 1/M_\infty$, and the static dielectric constant, $\varepsilon_S = 1/M_S$, are extracted from the intercepts of the semicircle at low and high frequency, respectively [58]. The values of ε_∞ and ε_∞ are used to calculate the dielectric strength, $\Delta\varepsilon$ [64,65,66].

A parameters M_∞, ε_∞, $\Delta\varepsilon$, τ_M and α are investigated and reported in Table 2 for temperature ranging from 303 to 373 K. The increase in ε_S with increasing in temperature at zero frequency, may be related to the well-known phenomenon that the polarization increases with temperature [67,68]. The calculated values of β and α reveal that; $\beta = (1-\alpha)$ [59]. The relaxation time is decreased due to the dipoles following the motion of the alternating field due to dissipated thermal energy [48].

4 Impedance formalism

For a polycrystalline dielectric material having interfacial boundary layers (grain-boundary), two semicircular arcs or depressed circular arcs may be obtained in the complex plane plot, which can be explained as two parallel RC elements connected in series as shown in Fig. 9(a), one branch is associated with the grain and other with the interfacial boundary of the sample. The real $Z^{'}(\omega)$ and imaginary $Z^{''}(\omega)$ of total impedance of the equivalent circuit are defined as [69]:

$$Z^{'}(\omega) = \left(\frac{R_g}{1+\omega_g^2 C_g^2 R_g^2}\right) + \left(\frac{R_{gb}}{1+\omega_{gb}^2 C_{gb}^2 R_{gb}^2}\right) + R_s \tag{15}$$

$$Z^{''}(\omega) = R_g\left(\frac{\omega_g C_g R_g^2}{1+(\omega_g C_g R_g)^2}\right) + R_{gb}\left(\frac{\omega_{gb} C_{gb} R_{gb}^2}{1+(\omega_{gb} C_{gb} R_{gb})^2}\right) \tag{16}$$

where R_g, R_{gb}, C_g and C_{gb} are the resistance and capacitance from the grain and grain boundary respectively, while ω_g and ω_{gb} are the frequencies at the peaks of the semi-circles for grain and grain boundary. The relative position of the two arcs in a complex plane can be identified by frequency. Generally, the arc of bulk lies in the frequency range higher than that of interfacial boundary since the relaxation time $\tau_M = 1/\omega_M$ for the interfacial boundary is much larger than that for the bulk crystal. Hence, when the bulk resistance, R_g, is much lower and the resistance in the equivalent circuit is dominated by the interfacial boundary resistance, R_{gb}, the arc of bulk (grain) may be masked in the limited frequency range [69,70]. The best fitting of RC equivalent at 303 K with one semi-circular arc of r_g= $(43.1 \times 10^3 \Omega)$ in the higher frequency region and a spike in the lower frequency region of r_{gb}(>90 MΩ) is shown in Fig. 9(a). In figures 9(b) and 9(c), the fitted data shows that as the temperature of annealing increases the value of the grain resistance decease and the effect of the grain boundary also decrease.

However, when R_{gb} becomes very high, the corresponding frequency f_M will be outside the limited frequency range and will show apart of grain boundary arc in Z^* plot. The parameters of interior grain such as R_g and C_g are estimated at the relaxation time $\tau_M = 1/\omega_M$ and reported in Table 2, but the parameters of the interfacial boundary were not estimated because of the limitation of the hardware of the bridge under 42 Hz and the accuracy of Cole-Cole diagram for $Z^*(\omega)$ will be out of the investigated experimental error. The previous presentation figures reveal that the impedance of grain and grain boundary decreases with the increase in temperature.

5 Impedance formalism

The plots of the real part of admittance, $Y^{'}(\omega)$=G_p, and the imaginary part of admittance, $Y^{'}(\omega)$=ωC_p , against are shown in Fig. 10. It can be assumed that series resistance Rs results from the resistance of electrodes. It is worth adding that contribution of R_s is noticeable in small-signal admittance (Fig. 10) only above 10^5 Hz and it found to be 269Ω, while for lower frequency (below 10^5 Hz) the small-signal admittance spectra are determined only by two elements, namely by

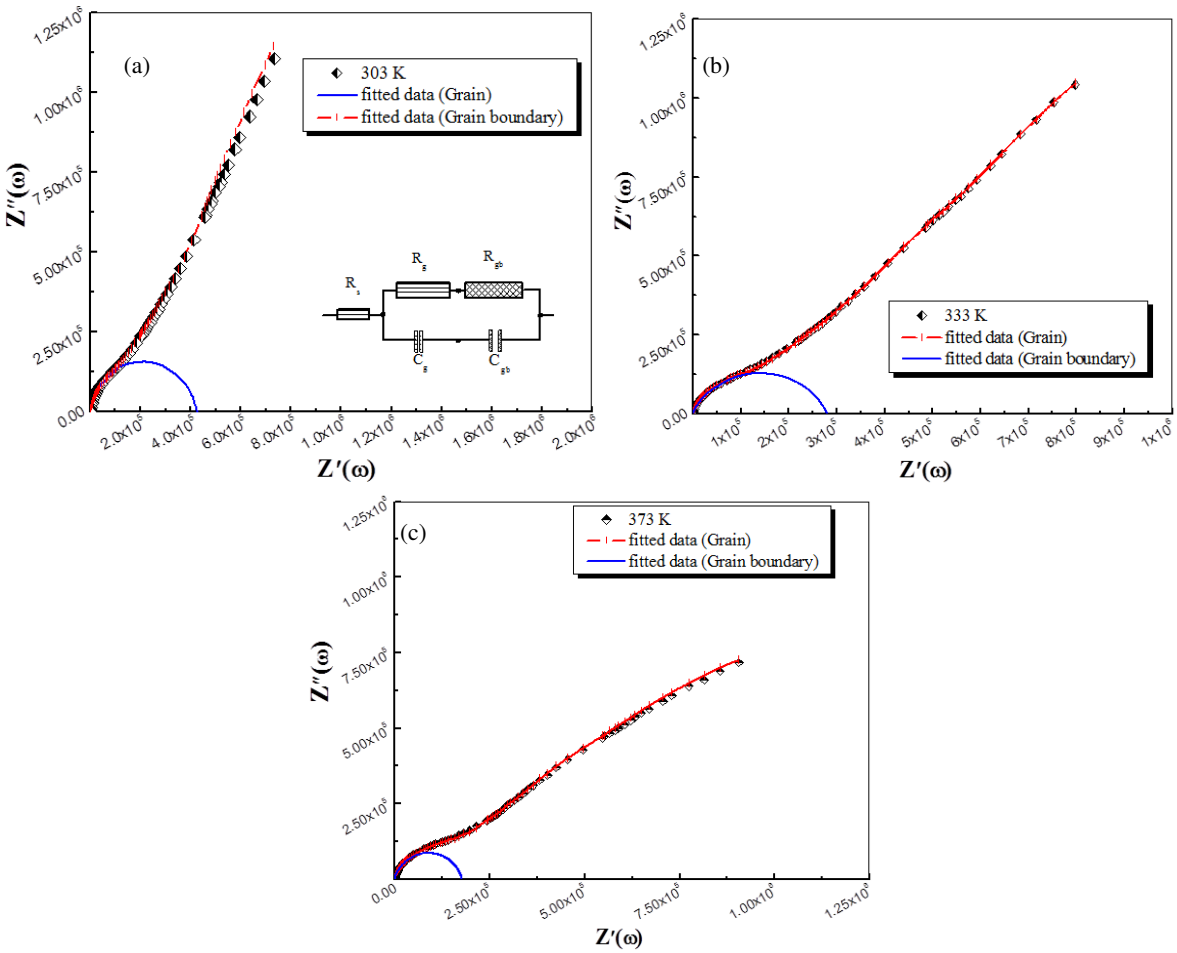

Fig. 9: Complex plane impedance plot of NiTPP films at (a) 303 K, 333 K, and 373 K, where (the solid line is the fitted data of RC equivalent circuit).

C and G (the part of the equivalent circuit restricted by the inset in Fig. 9(a)). The series resistance, Rs, in the equivalent circuit can be estimated also by using the fitting of Cole-Cole diagram at high frequency, which is found to be 270 Ω at room temperature. The investigated value of R_s for all prepared samples reveals that the resistance of each electrode will be $\approx$1/2 R_s $\approx$135$\approx$ and is independent of bias.

The observed symmetry of both curves indicates that both electrodes, namely the top and the bottom ones exhibit almost the same ability of charge injection. Smaller asymmetry can be referred to the fact that Au is nonreactive metal and the ration of roughness of the top electrode (or the length of in-diffusion of Au atoms) to the thickness of NiTPP (650 nm) is lower than that for the bottom electrode. In the work Kahn et al., [71] are discussing in details how the morphological difference between organic-on metal and metal-on-organic interfaces is reflected in the electrical characteristics of the contact.

6 Conclusion

The differential thermal analysis (DTA) measurement showed that the NiTPP has a thermal stability up to approximately 700 K. The value of sublimation temperature of NiTPP is 770 K. The Fourier transform infrared (FT-IR) technique in the range (4004000 cm^1) showed that the chemical structure of the powder, the as-deposited and annealed films are quit similar, so we can consider the thermal evaporation technique is a good one to obtain undissociated and stoichiometric NiTPP films. In lower and intermediate region of frequencies the real part of the dielectric decreases with the increase both of frequency and temperature but in MHz the temperature enhances the dielectric constant by a very small rate. The

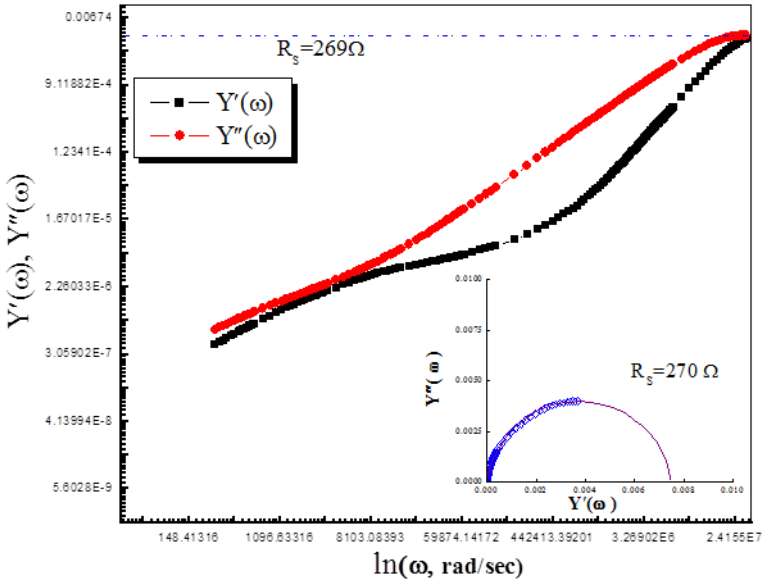

Fig. 10: The plots of for the real part of admittance and the imaginary part of admittance, versus logω. The inset shows the plots of the imaginary part of admittance, $Y^{'}(\omega)=\omega C_p$, and the real part of admittance, $Y^{'}(\omega)=G_p$, at room temperature in order to investigate the electrode resistance.

imaginary part of dielectric constant is found to decrease with the increase in frequency and increases with the increase in temperature in lower and intermediate frequencies. The analysis of the experimental results showed that the contribution of DC conductivity was eliminated at high frequencies larger than 200 KHz to 5 MHz region and the dielectric loss increases with frequency and decreases with increasing temperature. The calculated values of the maximum barrier height were found to be decreased from 0.37 to 0.27 eV as the temperature increased from 303 to 423 K. The analyzed experimental data of the ac conductivity for the prepared Au/NiTPP/Au showed three regions; the conduction mechanism in lower and intermediate frequencies corresponds to the correlated barrier hopping model but at higher frequencies the conduction mechanisms may be corresponded to the well-localized hopping and/or reorientational motion. The dielectric properties were analyzed via complex electric modulus formalism and the static dielectric constant was found to increase from 83.5 to 164.7 with temperature. The dynamic dielectric constant was found to decrease from 6.37 to 6 with increase in temperature. The Interior Grain parameters were investigated and the grain capacitance was found to increase from 1.89 to 3.9 nF and the grain resistance decrease from 215.4 to 88.1KΩ as the temperature increases from 303 to 373 K. The of admittance technique showed that the average value of the series resistance of the symmetric gold electrode is 269Ω.

References

[1] C. Castellarin Cudia, P. Vilmercati, R. Larciprete, C. Cepek, G. Zampieri, L. Sangaletti, S. Pagliara, A. Verdini, A. Cossaro, L. Floreano, A. Morgante, L. Petaccia, S. Lizzit, C. Battocchio, G. Polzonetti and A. Goldoni, Surf. Sci. 600 (2006) 4013
[2] J. Rogers, K. Nguyen, D. Hufnagle, D. Mc Lean, W. Su, K. Gossett, A. Burke, S. Vinogradov, R. Pachter and P. Fleitz, J. Phys. Chem. A 107 (2003) 11331.
[3] G. Hougham, G. Tesoro, A. Viehbeck and J. D. Chapple-Soko. Macromolecules; 27: (1994) 5964-71.
[4] M. D. Damaceanu, V. E. Musteata, M. Cristea and M. Bruma. Eur Polym J;46: (2010)1049-62.
[5] K. S. Cole, R. H. Cole, J. Chem. Phys. 9 (1941) 341.
[6] A. K. Jonscher, J. Mater. Sci. 16 (1981) 2037.
[7] R. Gerhardt, J. Phys. Chem. Solids, 55 (1994) 1491.
[8] M. Anwar and C. A. Hogarth J. Mater. Sci., 25 (1990) 3906
[9] P. Pissis, A. Kyritsis, Solid State Ionics 97 (1997) 105.
[10] X. Wei, X. Du, D. Chen, and Z. Chen, Thermochimica Acta 440 (2006) 181.
[11] G. L. Perlovich, O. A. Golubchikov and M. E. Klueva, J. Porphyrins Phthalocyanines 4 (2000) 699.
[12] Minerva Gamboa, Myriam Campos and Luis Alfonso Torres, J. Chem. Thermodynamics 42 (2010) 666.
[13] M. M. El-Nahass, H. M. Abd El-Khalek and A. M. Nawar, Optics Communications 285 (2012) 1872
[14] Xiao-Yuan and M.Z. Zgierski, J. Phys. Chem. 95 (1991) 4268.

[15] G. S. S. Saini, S. Sharma, S. Kaur, S. K. Tripathi, and C. G. Mahajan, Spectrochimica Acta A 61 (2004) 3070.
[16] S. Drr, U. Schade and P. Hellwig, Vibrational Spectroscopy 47 (2008) 59.
[17] O. K. Song, M.-J. Yoon, J.-R. Chang and D. Kim, Bulletin of the Korean Chemical Society 10 (1989) 35.
[18] M. M. El-Nahass, A. F. El-Deeb, H. S. Metwally and A. M. Hassanien, European Physical Journal Applied Physics 52 (2010) 10403.
[19] M. M. El-Nahass, H. M. Abd El-Khalek, and A. M. Nawar, Eur. Phys. J. Appl. Phys. (2012) 57: 30201
[20] N. G. McCrum, M.E. Read and G. Williams, Anelastic and dielectric effects in polymeric solids. London: John Wiley and Sons; (1967).
[21] Stefan Chisca, Valentina Elena Musteata, Ion Sava and Maria Bruma, European Polymer Journal 47 (2011) 1186.
[22] Siby Kurien, Jose Mathew, Shajo Sebastian, S. N. Potty and K. C. George, Materials Chemistry and Physics, 98 (2006) 470.
[23] Dev K. Mahato, AloDutta and T. P.Sinha, Physica B 406 (2011) 2703.
[24] R. M. Neagu, E. Neagu, N. Bonanos and P. Pissis, J. Appl. Phys. 88 (2000) 6669.
[25] M. Mei, Z. Lide and W. Guozhong, Nanostruct. Mater. 6 (1995) 823.
[26] E. Ikada, H. Fukushima and T. Watanabe J. Polym. Sci. Polym. Phys. Ed. 17 (1979) 1789.
[27] I. Ikada and M. Ashida, Colloid Polym. Sci. 264 (1986) 602.
[28] Z. W. He, C. M. Zhen, X. Q. Liu, W. Lan, D. Y. Xu and Y. Y. Wang, Thin Solid Films 462 (2004) 168.
[29] Arvind V. Sarode and Ashok C. Kumbharkhane, Journal of Molecular Liquids 160 (2011) 109.
[30] M. Meena and C. K. Mahadevan, Mater. Lett. 62 (2008) 3742.
[31] J. M. Stevels, Handbush der Physics, in: Flugge (Ed.), Springer, Berline, 1957, p. 350.
[32] U. Akgul, Z. Ergin, M. Sekerci and Y. Atici, Vacuum 82 (2008) 340.
[33] J. C. Giuntini, J. V. Zanchetta, D. Jullien, R. Eholie and P. Houenou, J. Non-Cryst. Solids 45 (1981) 57.
[34] T. T. Al-Dhhan and C. A. Hogarth, Int. J. Electron. 63 (1987) 707.
[35] R. D. Gould and A. K. Hassan, Thin Solid Films 223 (1993) 334.
[36] E. M. El-Menyawy, H. M. Zeyada and M. M. El-Nahass, Solid State Science, 12 (2010) 2182.
[37] H. M. Zeyada and M. M. El-Nahass, Appl. Surf. Sci. 254 (2008) 1852.
[38] Aleddin A. Saif and P. Poopalan, Journal of Alloys and Compounds, 509 (2011) 7210.
[39] S. Mahboob, G. Prasad and G. S. Kumar, Bull. Mater. Sci. 29 (2006) 347.
[40] A. A. Ahmed, Youssef and Z. Naturforsch. 57a (2002) 263.
[41] A. A. Atta, Journal of Alloys and Compounds, 480 (2009) 564.
[42] M. A. Afifi, A. E. Bekheet, E. Abd Elwahabb and H. E. Atyia, Vacuum 61 (2001) 9.
[43] J. M. Reau, X. Y. Jun, J. Senegas, Ch. Le Deit and M. Poulain, Solid State Ionics 95 (1997) 191.
[44] L. M. Hodge, M. D. Ingram and A. R. West, J. Electroanal. Chem. 74 (1976) 125.
[45] S.-A. Chen and C.-S. Liao, Macromolecules 26 (1993) 2810.
[46] R. Gerhardt, J. Phys. Chem. Solids 55 (1994) 1491.
[47] F. S. Howell, R. A. Bose, P. B. Macedo and C. T. Moynihan, J. Phys. Chem. 78 (1974) 639.
[48] F. Yakuphanoglu, I. S. Yahia, B. F. Senkal, G. B. Sakr and W. A. Farooq, Synthetic Metals, 161 (2011) 817.
[49] A. Mansingh, R. P. Tandon and J. K. Vaid, Phys. Rev. B21 (1980) 4829.
[50] F. S. Howell, R. A. Bose, P. B. Macedo and C. T. Moynihan, J. Phys. Chem. 78 (1974) 639.
[51] P. B. Macedo, C. T. Mognihan and R. Bose, Phys. Chem. Glasses 13 (1972) 171.
[52] P. Melnikov, C. Leon, J. Santamaria and F. Sanchez-Quesada, Journal of Alloys and Compounds 250 (1997) 520.
[53] I. M. Hodge, K. L. Ngai and C. T. Moynihan, Journal Of Non-Crystalline Solids, 351 (2005)104.
[54] K. S. Cole and R.H. Cole, J. Chem. Phys. 9 (1941) 341.
[55] D. R. Day, Y. J. Lewis, H. L. Lee and S. D. Senturia, J. Adhesion 18 (1985) 73.
[56] Y. Baziard, S. Breton, S. Toutain and A. Gourdenne, Eur. Polym. J. 24 (1988), 521.
[57] Y. Baziard, S. Breton, S. Toutain and A. Gourdenne, Eur. Polym. J. 24 (1988) 633.
[58] P. Hedvig, Dielectric Spectroscopy of Polymers (Adam Hilger, Bristol, 1977) P. 285.
[59] G. Perrier and A. Bergeret, J. Appl. Phys. 77 (1995) 2651.
[60] S. Selvasekarapandian, M. Vijaya Kumar, Journal of Materials Chemistry and Physics, 80 (2003) 29.
[61] Friedich Kremer and Andreas Schnhals (eds.), Broadband Dielectric Spectroscopy, Springer-Verlag Berlin Heidelberg, Germany, 2003, Chapter 3, pp.70-91.
[62] Evgenij Barsoukov, J. Ross Macdonald (eds), Impedance Spectroscopy Theory, Experiment, and Applications, 2nd edition, Published by John Wiley & Sons, Inc., Hoboken, New Jersey and Canada (2005), chapter 1, pp.17-20.
[63] M. El-Shabassy, A. S. Riad, Physica B, 222 (1996) 153.
[64] G. S. Nadkarni and J. G. Simmons, Journal of Applied Physics 41 (1970) 545.
[65] G. M. Tsangaris, G. C. Psarras and N. Kouloumbi, Journal of Materials Science 33 (1998) 2027.
[66] F. E. Salman and A. Mekki, Journal of Non-Crystalline Solids, 357 (2011) 2658.
[67] M. A. Ahamed, M. A. El-Hiti, M. K. El-Nimr and M.A. Kassem, J. Mater. Sci. Lett. 11 (1992) 1109.
[68] E. A. I. Saad, J. Optoelectro. Adv. Mater. 7 (2005) 3127.
[69] Pritam Kumar , B. P. Singh , T. P. Sinha and N. K. Singh, Physica B, 406 (2011) 139.
[70] Alo Dutta, Chandrahas Bharti and T. P. Sinha, Materials Research Bulletin, 43 (2008) 1246.
[71] A. Kahn, N. Koch and W. Gao, J. Polym. Phys. B 41 (2003) 2529.